Magnetic fields beneath active region coronal loops

Philip G. Judge,[1] L. Kleint,[2] and C. Kuckein[3]

[1] *Visitor, Astronomical Institute of the University of Bern, Sidlerstrasse 5, 3012 Bern, and*
High Altitude Observatory, National Center for Atmospheric Research, Boulder CO 80307-3000, USA
[2] *University of Bern, Astronomical Institute, Sidlerstrasse 5, 3012 Bern, Switzerland*
[3] *Leibniz-Institut für Astrophysik Potsdam (AIP), An der Sternwarte 16, 14482 Potsdam, Germany*

ABSTRACT

We examine the hypothesis that multipolar magnetic fields advected by photospheric granules can contribute heating to the active chromosphere and corona. On 28 September 2020 the GRIS and HiFI+ instruments at the GREGOR telescope obtained data of NOAA 12773. We analyze Stokes profiles of spectral lines of Si I and He I, to study magnetic fields from photosphere to the upper chromosphere. Magnetogram and EUV data from the HMI and AIA instruments on the SDO spacecraft are co-aligned and studied in relation to the GRIS data. At coronal loop footpoints, minor polarity fields comprise just 0.2% and 0.02% of the flux measured over the $40'' \times 60''$ area observed in the photosphere and upper chromosphere, centered $320''$ from disk center. Significantly, the minority fields are situated $\gtrsim 12''$ from bright footpoints. We use physical arguments to show that any unresolved minority flux cannot reach coronal footpoints adjacent to the upper chromosphere. Even if it did, the most optimistic estimate of the energy released through chromospheric reconnection is barely sufficient to account for the coronal energy losses. Further, dynamical changes accompanying reconnection between uni- and multi- polar fields are seen neither in the He I data nor in narrow-band movies of the Hα line core. We conclude that the hypothesis must be rejected. Bright chromospheric, transition region and coronal loop plasmas must be heated by mechanisms involving unipolar fields.

Keywords: Solar corona

1. INTRODUCTION

Many mechanisms for driving the heating and dynamics of corona plasma have been proposed since Edlén (1943) first proved that the plasma temperature exceeds that of the Sun's surface by a factor of at least fifty. The problem is multi-faceted and it has resisted definitive solution for a variety of good physical reasons (highlighted recently by Judge & Ionson 2024). The problem can be usefully divided into three parts: what is the nature of the source of upwardly propagating energy? How does the energy propagate through the atmosphere? How is this energy transformed irreversibly into heat? The purpose of the present paper is to examine the generation of magnetic energy via the evolving magnetic field immediately beneath the corona.

A significant fraction of heating mechanisms invoke the generation of upward-directed magnetic energy through the interaction and reconfiguration of small-scale magnetic fields which are advected by photospheric granular flows. These flows can generate Poynting fluxes of electromagnetic energy both steadily, as the emerging magnetic bundles of flux are entwined around each other (Parker 1972, 1988; Pontin & Hornig 2020), as MHD waves are generated (Osterbrock 1961; Uchida & Kaburaki 1974; Hollweg 1978; Howson et al. 2020), and as magnetic reconnection beneath the corona causes bulk fluid flows, small flares and related phenomena (e.g. Sturrock 1968; Shibata et al. 2007; Nelson et al. 2019; Carlsson et al. 2019).

Proposals involving magnetic reconnection of rapidly evolving granular fields (Lin & Rimmele 1999) with long-lived supergranular network boundary fields (Leighton 1959; Leighton et al. 1962) have formed the basis of mod-

Corresponding author: Philip G. Judge

els of coronal heating for several decades. Title & Schrijver (1998) suggested that magnetic reconnection driven by granular convection, observed as a "magnetic carpet" of continuously evolving photospheric fields being replaced about once per day, naturally leads to overlying coronal heating. The idea continues to stimulate later work (e.g. Schrijver et al. 1998; Priest et al. 2002; Wang 2016; Chitta et al. 2017, 2023). A search for the term "magnetic carpet" along with "corona" in the NASA ADS database reveals over 60 diverse abstracts using this concept. Related is the concept of "interchange reconnection", frequently advocated to explain both the evolution of coronal hole boundaries, and as a power source for the solar wind (Nash et al. 1988; Fisk 2003). In all such studies, a direct connection is made between observed mixed polarity photospheric magnetic fields and heating of the corona. Here we examine this picture for active region loops which result from the most intense form of coronal heating. While magnetic fields at loop footpoints are locally almost unipolar (Giovanelli 1980), the magnetic carpet picture nevertheless continues to be considered viable there (Priest et al. 2002, 2018; Chitta et al. 2017, 2023).

The primary difference of the present article with earlier work is in use of measurements of chromospheric magnetic and velocity fields to assess coronal heating mechanisms. Chromospheric heating has recently been analyzed using GREGOR data similar to those analyzed here by Anan et al. (2021).

2. OBSERVATIONS

Here we examine datasets obtained using the GRIS instrument (Collados et al. 2012) from the GREGOR telescope (Schmidt et al. 2012; Kleint et al. 2020) augmented by narrow-band images in the Hα line core and continuum from the HiFI+ instrument (Denker et al. 2023). Standard products from HMI and AIA were used to define the frame of reference and to compare with images of the heated plasma above. The field-of-view observed by the GRIS instrument is shown as a rectangle in Figure 1. GRIS is a scanning slit spectropolarimeter, which builds up an image of the solar spectrum in the four Stokes parameters I, Q, U and V by letting light pass through a slit to a diffraction grating. The dispersed spectra were focused for each polarization state on a 2D detector, with wavelength in the dispersion direction, and position along the 1D slit perpendicular to this. The slit was moved in 300 steps of $0.''135$ across the solar image to build up a scan over 29 minutes and 30 seconds with a field of view (FOV) of 40.5 x 59.8 arcsec. Examples of the level-1 data acquired are shown in Figure 2.

When reduced to a level-1 data product, data cubes of the form

$$S(x, y, \lambda, i), \tag{1}$$

are constructed, functions of the two spatial pixels (x, y) on the Sun, wavelength λ and one of the four polarization states labeled with index i.

2.1. GRIS observations from September 28 2020

Table 1 lists properties of the two GREGOR instruments with data analyzed here. From Figure 1, the HMI data reveal that GRIS scanned just one major polarity of the active region NOAA 12773, the strongest then on the solar disk. Figure 3 displays line-of-sight ("LOS") magnetic flux densities and velocities, both along the LOS, for the photospheric line of Si I (left) and chromospheric line of He I (center) respectively. These were derived using same procedures as in the paper by Judge et al. (2024). The magnetic LOS fluxes, derived from the weak field approximation applied to the I and V Stokes profiles of both lines, are listed in Table 2. The effective Landé g-factors used for 1082.7 and 1083.0 lines of Si I and He I were 1.58 and 1.25 for longitudinal Zeeman components, respectively, and 2.45 and 1.53 for the transverse components.

The magnetic sensitivity of HMI to LOS fields is roughly $\sigma(B_{\rm LOS}) \equiv 10$ Mx cm^{-2}, which gives 2.6×10^{16} Mx for each $0.504'' \times 0.504''$ pixel (Liu et al. 2012). In contrast, that of the GRIS observations for the 1082.7 nm line of Si I is $\sigma(B_{\rm LOS}) \sim 3.3$ Mx cm^{-2} measured from high frequency noise of the derived $B_{\rm LOS}$ data themselves. The projected GRIS pixel areas are $0.135'' \times 0.135''$, leading to a sensitivity of LOS photospheric fluxes of $\sim 3 \times 10^{14}$ Mx. For the chromospheric He I line, the sensitivities were measured to be three times larger than measured for the Si I line.

Figure 3 displays two contours of LOS magnetic flux density, the blue contour traces a value of $+6$ Mx cm^{-2}, the black contour a value of -150 Mx cm^{-2}. Taken together with Figure 1, it is evident that GRIS measured magnetic properties at the footpoints of a group of coronal loops, themselves extending across this active region roughly from $X = 0, Y = 320$ to $X = -100$ and $Y \approx 350 - 410$. From Figure 3 and Table 2 we note, in particular:

- GRIS detects 1.7× more photospheric LOS flux than HMI. We believe this difference reflects the higher sensitivity and angular resolution achieved by GRIS during the raster scan.

- Less than 0.2% of the photospheric magnetic flux covering this area is of opposite polarity.
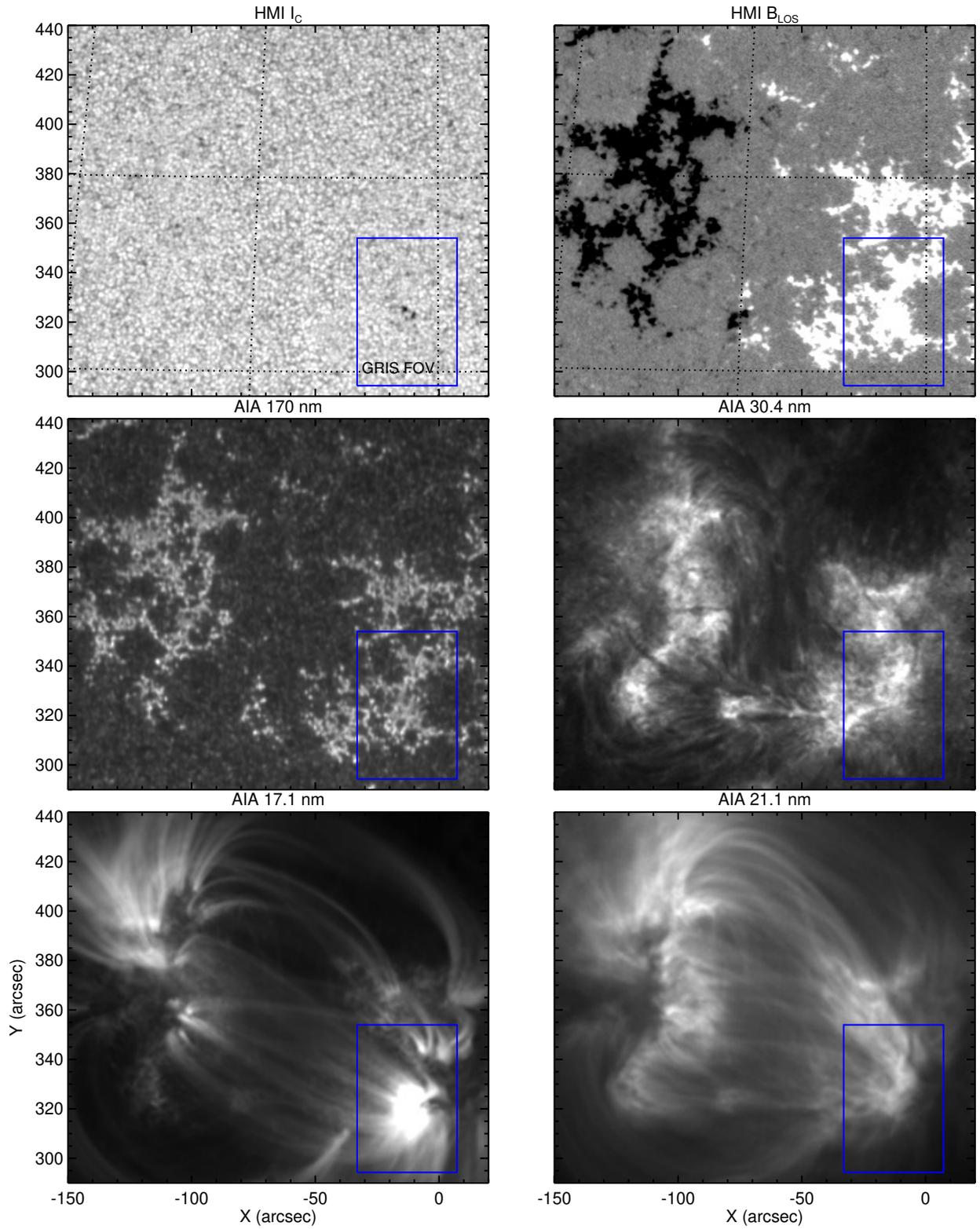
Figure 1. Images are shown from the SDO spacecraft obtained near 19:41 UT on 28 September 2020, the mid-time of the scan with GRIS, of the active region NOAA 12773. The field of view scanned by the GRIS is indicated as a blue rectangle. The slit was oriented 2.4 degrees clockwise from the N-S direction, and the slit scanned in the E-W direction. North is upwards in the figure.
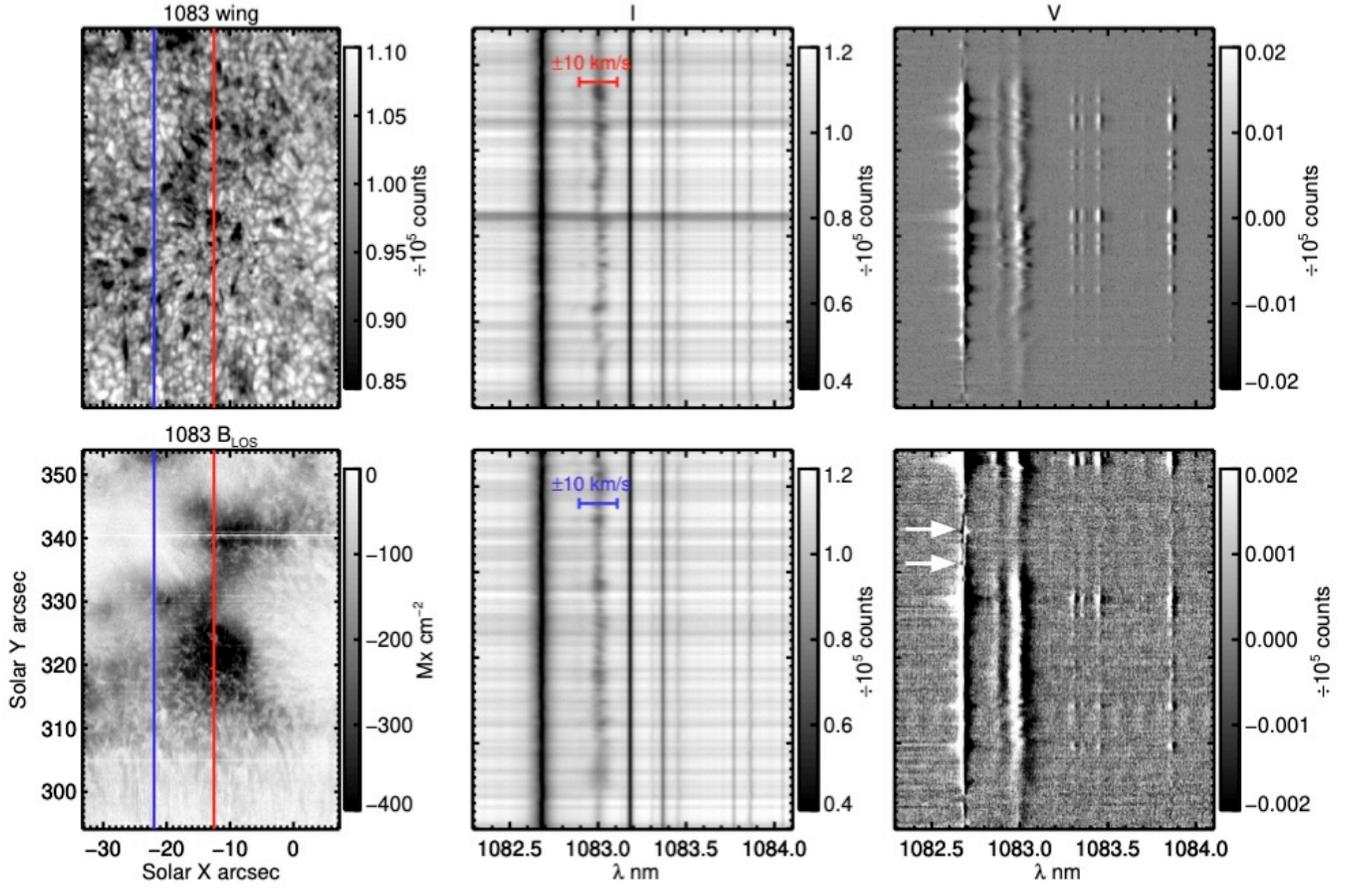
Figure 2. Images show line wing intensity and derived LOS magnetic flux density (left panels), and spectra of intensity (middle panels) and circular polarization (right panels), from active region NOAA 12773. The four spectra are taken from the red and blue vertical slit positions shown in the left panels, the upper rows are from the red position, the lower from the blue. The I and V images are in units of 10^5 counts. The Stokes V profiles in the bottom right panel show two regions of minority polarity in the Si I 1082.7 nm line beneath the majority polarity of the He I 1083 nm line, indicated by white arrows.

Table 1. GREGOR observations examined from September 28 2020

Instrument	Mode	Start	End	Cadence	FOV	spatial	detector	λ	$\Delta\lambda$
		UT		s	arcsec	pixel$''$	format	nm	
GRIS	IQUV	09:27:01	09:56:24	5.9	$40.5^* \times 59.8$	0.135	443×1010	1082.322-1084.136	0.018
							(solar Y $\times \lambda$)		
HiFI+ No.2	I	08:26:38	10:34:33	6	76.5×60.5	0.0498	1536×1216	656.279	0.060

*Slit is $59\rlap{.}''8$ long, $40\rlap{.}''5$ equals 300 steps of $0\rlap{.}''135$ in solar X (E-W direction).
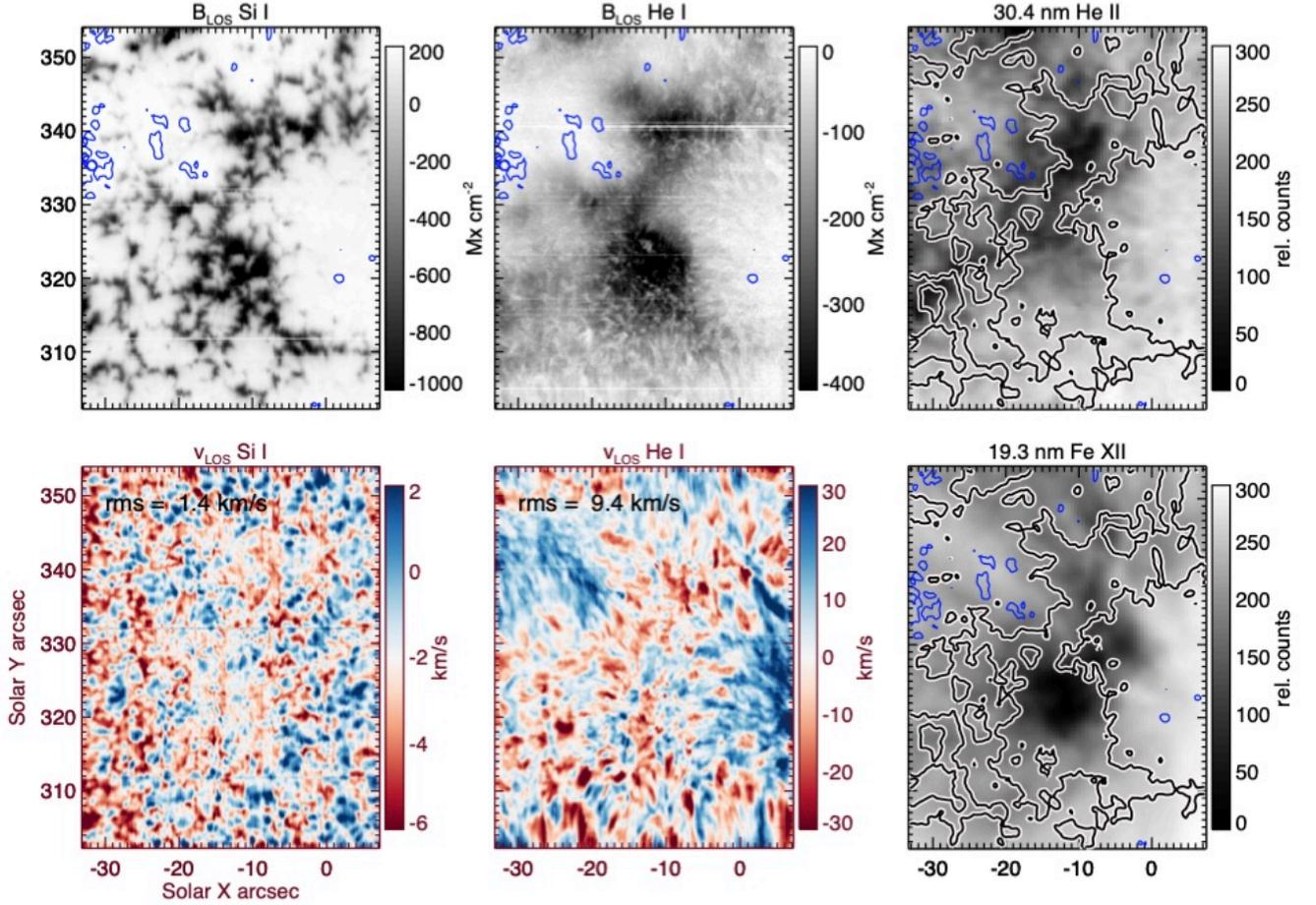
Figure 3. Images of active region NOAA 12773 on September 28 2020 spanning the area scanned by GRIS are shown. Top row: LOS photospheric magnetic field, LOS chromospheric magnetic field, and intensity of the 30.4 nm channel of AIA. Bottom row: LOS Doppler shifts of the cores of Si I and He I lines, and the intensity of the 19.3 nm channel of AIA. Doppler shifts are shown in red and blue (away from and towards the observatory). The color table of the AIA data is reversed (i.e., dark = brighter emission), superposed with photospheric GRIS B_{LOS} contours at +6, -150 Mx cm^{-2} in blue and black respectively. Blue contours are also shown in the uppermost panels.

- But less than 0.02% of the chromospheric magnetic flux is of minority polarity.

- Doppler shifts of the He I line core have amplitudes typically $\lesssim$ 10 km s^{-1} (Figures 2 and 3).

2.2. *HiFI+ data*

Simultaneously with the GRIS observations, narrowband images of the core of the Hα lines at 656.3 nm were obtained using HiFI+ (Table 1). These data were acquired in rapid bursts, reduced with the software package `sTools` (Kuckein et al. 2017) and reconstructed using the multi object multi-frame deconvolution algorithm (MOMFBD, Van Noort et al. 2005), and co-aligned to

sub-pixel precision. The average of all such images between 09:27 and 09:55 UT were then co-aligned with the He I GRIS images of line core intensity, line width and Doppler shift. Hα core intensity images are naturally quite different from these GRIS images. However we are certain of this multi-instrument co-alignment to a precision of $\pm1''$ because there are several features in common in both sets of images. Two such images can be found below (Figures 4 and 5).

3. ANALYSIS

The above data are well matched to test the hypothesis that multipolar photospheric magnetic fields influence coronal heating. The first challenge to this idea is

Table 2. Statistics of LOS magnetic fluxes within the region scanned by GRIS

λ	Ion	Instr.	$-$ve flux	$+$ve flux	$+$ve $\div$
nm			Mx	Mx	$-$ve
617.3	Fe I	HMI*	$-1.2(21)^{\dagger}$	7.6(18)	-0.006
1082.7	Si I	GRIS	-2.0(21)	4.0(18)	-0.002
1083.0	He I	GRIS	-1.1(21)	2.6(17)	-0.0002

*The 45s data product was used in this article. †The notation is such that $7.6(18) \equiv 7.6 \times 10^{18}$. The area scanned by GRIS, analyzed in common with HMI, is 1.3×10^{19} cm^2. The flux sensitivities of the measurements of the three lines listed are 3×10^{16}, 3×10^{14}, and 10^{15} Mx respectively.

the dramatic imbalance between major and minor polarity photospheric fluxes. Similar to five other areas observed with the ViSP instrument on the DKIST (Judge et al. 2024; Judge & Kuin 2024), the minor polarity flux measured is just 0.2% of the entire flux. In the chromosphere this fraction drops by a factor of 10. In an appendix, Judge & Kuin (2024) present physical arguments as to why opposite polarity flux cannot simply be hidden as a result of cancellation of V signals in the low β environment of the upper chromosphere. The second important point is that minor polarity fields should be found geometrically close to footpoints of coronal plasma loops. From Figure 3 (bottom right panel) we see that the opposite polarity flux lies about 10 Mm from the nearest bright coronal plasma. The white arrow in Figure 2 indicates clearly a minority polarity signature in the photosphere that is absent in the chromospheric data. Opposite polarity fields do not reach the chromospheric formation height of He I 1083 nm. Further, the chromospheric "fibrils" clearly traced by the Doppler shifts of the He I lines (below $Y = 303$ in the lower middle panel of Figure 3) clearly lie above multiple concentrations of minority polarity flux.

The image of B_{LOS} of the He I line contains several kinds of structures at the resolution of ≈ 200 km: the dense cores of strong fields appear uniform. Around these are mottled region (see the gray-white patterns near $Y = 310''$ in Figure 2). Then there are signatures of chromospheric fibrils most readily seen at $Y < 307''$. These regions are all unipolar. The mottle pattern has a characteristic scale of about $2'' \equiv 1.5$ Mm. There is, however, no significant correlation with granulation patterns in the continuum observed simultaneously with GRIS (Kendall's rank correlation coefficient τ is just 0.16 with a probability of correlation of zero).

Are these minor polarity fields important for forming the transition region? Supporting evidence would sug-

gest the presence of "cool loops" as a basic structure for the transition region](e.g. Hansteen et al. 2014), extended to these otherwise unipolar regions. The upper right panel of the figure shows that, if anything, the largest opposite polarity patches of flux lie where the 30.4 nm line of He II is weak. Other areas of strong He II emission are associated far more with the unipolar dominant field than anything related to the minority flux.

3.1. *Consequences of reconnection of opposite polarity fields with the magnetic network*

If significant, reconnection between granular and network fields must be accompanied by observable plasma motions somewhere within chromospheric plasma. Reconnection is intrinsically faster as the Alfvén speed increases, and so is the subsequent plasma dynamics. Hence any reconnection outflows driven by newly unbalanced Maxwell stresses should be observed mostly in the upper chromosphere where the plasma inertia is small. Changes in magnetic connectivity manifested through fibril structures should also be observed as a consequence of the proposed mechanism, as the system seeks a lower energy configuration after reconnection (e.g. Kulsrud 2011). The central region of Figure 3 hosts the brightest coronal emission. This region is completely unipolar as detected by GRIS. The LOS Doppler shifts are unexceptional, rms speeds on the order of the chromospheric sound speed $c_{\mathrm{S}} \lesssim 10$ km s^{-1} in the regions under bright coronal emission. In the photosphere, where $\rho \approx 10^{-7}$ g cm^{-3} and $B \gtrsim 300$ G (measured in the Si I line), the Alfvén speed is $c_{\mathrm{A}} \gtrsim 3$ km s^{-1}. Reconnection in the photosphere is very slow. But through the chromosphere, ρ decreases exponentially with height to $\sim 10^{-13}$ g cm^{-3}. With $B \sim 200$ G, estimated from the He I 1083 nm line, c_{A} exceeds 800 km s^{-1}. There is no evidence of speeds remotely approaching such values in the regions below coronal footpoints in the figures here or those in Judge et al. (2024). Observed chromospheric rms speeds are almost two orders of magnitude smaller (Figure 3).

We have searched for morphological changes in fibrils in Hα data from the HiFI+ instrument (Table 1). Figures 5 and 6 show snapshots and a 6 second cadence movie of the region directly beneath the bright coronal emission. The movie is included as online material. These data reveal that any on-going reconnection on observable scales lies below the detection limit of changes in magnetic fields and fluid motions, both Doppler and proper motion signatures.

The qualitatively similar observations of Díaz Baso et al. (2021) were of an initially unipolar pore, but with a clearly observable emerging region of opposite polar-

ity and spanning several arcseconds nearby. Over several hours they measured a reduction in flux of 4×10^{19} Mx of both polarities. These fluxes are an order of magnitude higher than the minor polarity flux in the far more unipolar region reported here (Table 2). This flux "cancellation" (a descriptive not a physical term) was accompanied by ongoing bright chromospheric emission, some coronal emission, increasing transverse magnetic fields, falling longitudinal fields, and images of plasmoids moving with speeds of $\sim 10^2$ km s^{-1}. None of these phenomena are present in the data analyzed here.

3.2. *Hidden minority fields in otherwise unipolar regions*

Figures 3–5 highlight the resolved minority polarity regions using blue contours for small values of $|B_{\mathrm{LOS}}|$, the other contours show regions of dominant polarity at much larger values of $|B_{\mathrm{LOS}}|$. The small areas of fields of minority polarity are observed away from the dominant polarity network regions by at least $2''$.

Some have argued that minority-polarity features, if small, can lie undetected *within or adjacent to* network patches of dominant polarity, in the photosphere. Here we examine the consequences of the proposition that such fields extend into the *chromosphere* and above.

For decades, this effect has been recognized in photospheric measurements (Stenflo 1973). Unresolved structure contributing to the net Stokes V profiles are described by a "filling factor" of the dominant unresolved magnetic field. But in the upper chromosphere the magnetic filling factor is close to one. We estimate the plasma β to be $\lesssim 0.001$ where the He I lines form (Avrett et al. 1994), thus no force can counteract an imbalanced Lorentz force. The plasma is almost force-free, filling the volume with magnetic field. If the chromospheric plasma were not force-free, it would evolve at the Alfvén speed to make it so. Any minority flux concentration must therefore also have $B \sim 200$ G, the pressure being constant across any mis-aligned vector magnetic fields. To be absent from the chromospheric measurements of B_{LOS} presented here, it must lie below a 3σ sensitivity $\approx 3 \times 10^{15}$ Mx. With $B \sim 200$ G, the minor polarity flux must occupy an area $A \lesssim 5 \times 10^{12}$ cm^2, equivalent to a square of 22 km on a side, subtending an angle of $0''\!.03$ at the Sun, four times smaller than the GRIS pixel size. We can estimate the energy released by the complete annihilation of these fields with the network field. The geometry is represented by the cartoon shown as Figure 11 of Díaz Baso et al. (2021). When this field is advected to the network at speed $u \sim 0.5$ km s^{-1}, the total power entering the diffusion region from both sides is

$$2\frac{B^2}{8\pi}\frac{\ell u}{\sqrt{A}} \approx 10^9 \quad \text{erg cm}^{-2}\text{ s}^{-1} \tag{2}$$

over the vertical area A, where we have taken $\sqrt{A}$ as the horizontal transverse size of the advected flux bundle and $\ell \sim 150$ km as the vertical size of the reconnecting diffusion region. For ℓ we use the scale height at the top of the chromosphere where reconnection is fastest. This energy flux density can be compared with 1.6×10^8 erg cm^{-2} s^{-1} estimated for the energy released from a much larger region of the chromosphere via reconnection by Díaz Baso et al. 2021. Clearly equation (2) is a gross overestimate, the maximum available power in reconnection which must be averaged over an entire GRIS pixel of $0''\!.135$ on a side, a horizontal area twenty times larger. Further, initially just one half of the energy of reconnection travels upwards, and of this, at most half ultimately will end up as plasma heating (reconnection leads initially to bulk acceleration, only consequent processes lead to irreversible heating). Taking these factors into account, an upper limit to the flux density of energy available for heating per unit area is $\lesssim 1.3 \times 10^7$ erg cm^{-2} s^{-1}. This is similar to the required flux density of 10^7 erg cm^{-2} s^{-1} (Withbroe & Noyes 1977). The proposal is tenable in terms of energy, but only barely, and even then it requires fully half of the available upward directed energy to be converted into heat. Any misalignment of reconnected fields from anti-parallel reduces this estimate further.

Lastly, in their appendix, Judge & Kuin (2024) argued independently that such fields would be incompatible with observations and force balance in the low plasma-β upper chromosphere.

4. CONCLUSIONS

In summary, nothing about the dataset analyzed suggests a role for the small-scale multipolar granular fields in coronal heating, contrary to the findings of papers based upon photospheric magnetic field measurements (Priest et al. 2002, 2018; Chitta et al. 2017, 2023), but in agreement with our work using different chromospheric magnetic field measurements (Judge et al. 2024; Judge & Kuin 2024). The differences can perhaps be reconciled because chromospheric measurements are superior to photospheric measurements for investigating conditions at the coronal base. Our work is magnetically far more sensitive than earlier work, for instance with MDI (Schrijver et al. 1998) or HMI (Wang 2016) instruments. The diagnostic He I multiplet cannot form deeper than the uppermost scale height of the chromosphere, it either forms there via the penetration of EUV photons from the hotter plasma above, or it is essentially absent
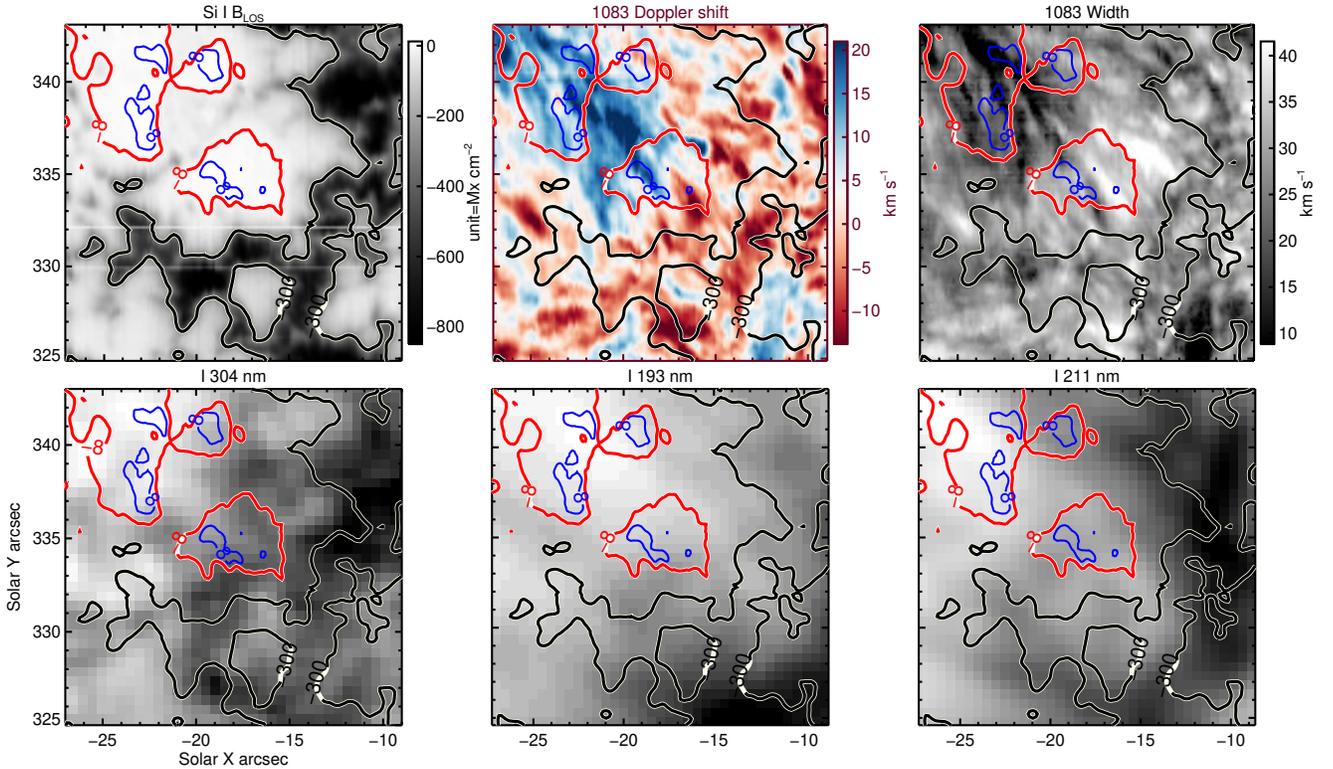
Figure 4. Minor polarity photospheric magnetic flux is highlighted within blue contours (8 Mx cm^{-2}) together with majority polarity contours at -8 (red) and -300 Mx cm^{-2} (black). In the top row the images show LOS photospheric magnetic flux density (left panel), He I 1083 nm Doppler velocity density (middle panel), and width (right panel). AIA data are shown in the lower three panels, darker image density means brighter emission. The minor polarity photospheric flux patches are encircled by major polarity flux, and exhibit no correlations with any of the features formed in the upper chromosphere (He I properties or above (AIA brightnesses).

(Avrett et al. 1994; Leenaarts et al. 2016). It seems to us that earlier work based on photospheric magnetic fields, including those using sophisticated extrapolation schemes, simply cannot offer the kind of penetrative diagnostics available to ground-based polarimetry of chromospheric plasmas.

Signatures of magnetic reconnection between observed minor polarity fields (blue contours in the figures), and the dominant fields are simply not observed. Together with physical arguments against multipolar chromospheric fields above plages (section 3.2), we suggest that reconnection in chromospheric plasma directly beneath typical active region loop footpoints does not play a role in heating the loops. We conclude that, along with a study of the 854.2 nm line of Ca II observed with DKIST reported by Judge et al. (2024), there is less and less room available to believe that opposite polarity fields have a role to play in heating the active corona. This conclusion calls into question the role of the "magnetic carpet" in the heating of active coronal loops, (Title & Schrijver 1998; Priest et al. 2002). This refutation,

if confirmed, marks a significant advance in the quest to identify heating mechanisms by eliminating an entire class of energy sources for commonly observed plasma loops (Judge & Ionson 2024).

It will be interesting to explore the kinds of observations presented here with other datasets, especially in regions of quiet Sun where, although the He I lines are weak, they can still be used to probe conditions at the coronal base (Harvey & Hall 1971; Rüedi et al. 1996; Lagg et al. 2004). In the case that the He I lines are too weak to explore at sufficiently high angular resolution, one might use the 854.2 nm line of Ca II, or if selected for flight, various lines of Mg II and Fe II in the UV region (259-281 nm) using the Chromospheric Magnetism Explorer instrument (Gilbert & CMEx Team 2023, see Judge et al. 2021, 2022 for reasons to observe in this region).

Based upon the observations presented here and elsewhere (Judge et al. 2024; Judge & Kuin 2024), we wish to make a final remark on the well-known dynamics and thermal fine structure in the chromosphere. In this con-
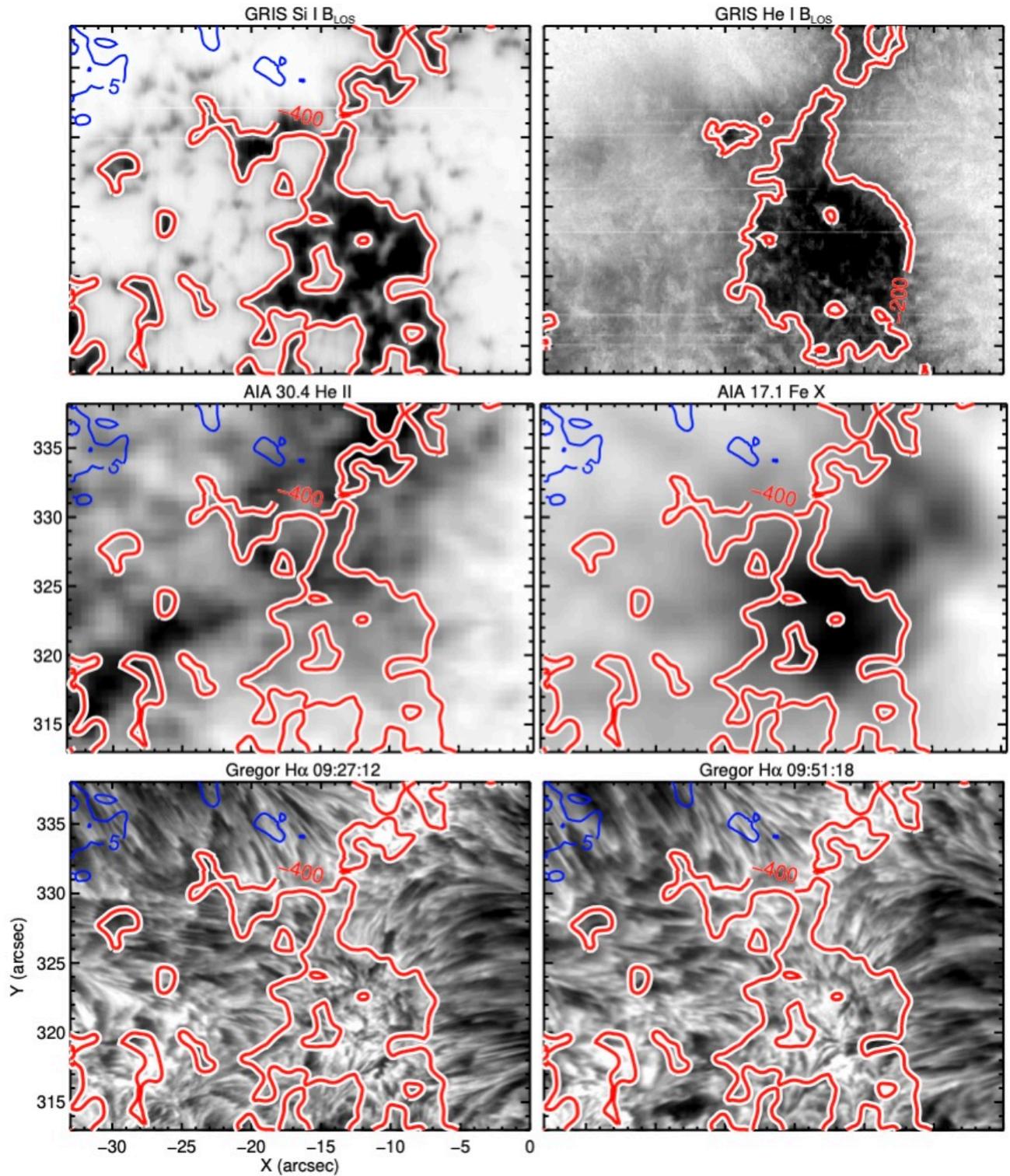
Figure 5. A close view of chromospheric magnetic field, AIA images and Hα images from the HiFI+ instrument on GREGOR. The two Hα images, separated by 24 minutes, show a similar morphology, with fibrils frequently aligned nearly perpendicular to the -400 Mx cm^{-2} contour (red/white) of photospheric magnetic fields.

text, we are struck by the fact that the dynamics appear to reflect mostly field-aligned motions (see Figure 6), as changing pressures associated with granulation drive fluid into the chromosphere, which mostly returns downwards. Such motions do little work on magnetic fields. Instead it is likely that much of this eye-catching dynamics is associated with pressure-driven sonic flows (e.g. Hansteen et al. 2006, who studied such motions in the context of "spicules of type I"). They are highly visible because of associated variations in density and temperature. Yet such motions cannot significantly influence coronal heating, through the same argument used by Athay & White (1978) to deny acoustic waves a role in heating the corona. In essence, unless there is clear evidence for reconnections and/or cross-field plasma acceleration driven by flux emergence, the dynamic fine structure of the chromosphere is of no real interest for heating the corona. The more supersonic spicules of "type II" could in principle supply kinetic energy into the corona (de Pontieu et al. 2007), but perhaps the area covered by them too small to explain the rather "thick" coronal loops and quieter regions which seem to be larger

across the dominant direction of the magnetic field (even the thinnest coronal structures yet found seem to exceed 250 km, Rachmeler et al. 2022). The product of their number times surface area (in the traditional interpretation of thin, straw-like structures) is far smaller than the area of the corona, and given the frozen-field condition, so it is difficult to see how they might transfer energy across magnetic fields to fill the larger coronal volume. It may be useful to keep this observation in mind when discussing coronal heating and dynamics, perhaps by trying to identify where the chromospheric dynamics does work on the magnetic field extending into the corona.

ACKNOWLEDGMENTS

REFERENCES

Anan, T., Schad, T. A., Kitai, R., et al. 2021, ApJ, 921, 39, doi: 10.3847/1538-4357/ac1b9c

Athay, R. G., & White, O. R. 1978, ApJ, 226, 1135

Avrett, E. H., Fontenla, J. M., & Loeser, R. 1994, in Infrared Solar Physics, ed. D. M. Rabin, J. T. Jefferies, & C. Lindsey, Proc. IAU Symp. 154 (Dordrecht: Kluwer), 35–47t

Carlsson, M., de Pontieu, B., & Hansteen, V. H. 2019, Ann. Rev. Astr. Astrophys., 57, 189

Chitta, L. P., Peter, H., Solanki, S. K., et al. 2017, ApJS, 229, 4, doi: 10.3847/1538-4365/229/1/4

Chitta, L. P., Solanki, S. K., del Toro Iniesta, J. C., et al. 2023, ApJL, 956, L1, doi: 10.3847/2041-8213/acf136

Collados, M., López, R., Páez, E., et al. 2012, Astronomische Nachrichten, 333, 872, doi: 10.1002/asna.201211738

de Pontieu, B., McIntosh, S., Hansteen, V. H., et al. 2007, PASJ, 59, 655

Denker, C., Verma, M., Wiśniewska, A., et al. 2023, Journal of Astronomical Telescopes, Instruments, and Systems, 9, 015001, doi: 10.1117/1.JATIS.9.1.015001

Díaz Baso, C. J., de la Cruz Rodríguez, J., & Leenaarts, J. 2021, A&A, 647, A188, doi: 10.1051/0004-6361/202040111

Edlén, B. 1943, Zeitschrift für Astrofysik, 22, 30

Fisk, L. A. 2003, Journal of Geophysical Research (Space Physics), 108, 1157, doi: 10.1029/2002JA009284

Gilbert, H., & CMEx Team. 2023, in AAS/Solar Physics Division Meeting, Vol. 55, AAS/Solar Physics Division Meeting, 304.01

Giovanelli, R. G. 1980, Sol. Phys., 68, 49

Hansteen, V., de Pontieu, B., Carlsson, M., et al. 2014, Science, 346, 1255757

Hansteen, V. H., de Pontieu, B., Rouppe van der Voort, L., van Noort, M., & Carlsson, M. 2006, ApJL, 647, L73

Harvey, J., & Hall, D. 1971, in Solar Magnetic Fields, ed. R. Howard, Vol. 43, 279

Hollweg, J. V. 1978, Sol.Phys, 56, 305, doi: 10.1007/BF00152474

Howson, T. A., de Moortel, I., & Reid, J. 2020, A&A, 636, A40

Judge, P., Bryans, P., Casini, R., et al. 2022, ApJ, 941, 159, doi: 10.3847/1538-4357/aca2a5

Judge, P., Kleint, L., Casini, R., et al. 2024, ApJ, 960, 129

Judge, P., Rempel, M., Ezzeddine, R., et al. 2021, ApJ, 917, 27

Judge, P. G., & Ionson, J. A. 2024, The Problem of Coronal Heating. A Rosetta Stone for Electrodynamic Coupling in Cosmic Plasma (Springer, in press, March 2024)

Judge, P. G., & Kuin, N. P. M. 2024, ApJ

Hα core 28 Sep 2020 09:27 - 09:55 UT
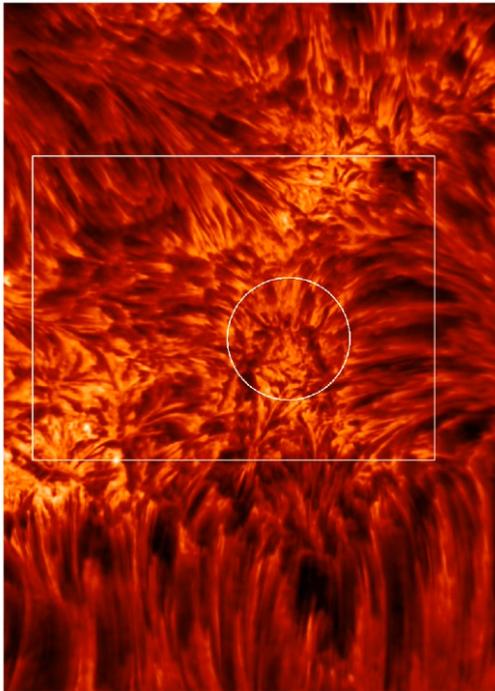
Figure 6. A snapshot of a movie of Hα images from the HiFI+ instrument on GREGOR is shown. The online movie shows a frame every 6 seconds for 28 minutes. The movie shows mostly signatures of flows along the long striation patterns. The box shows the area scanned by the GRIS instrument, and the circle highlights the footpoint of the most intense EUV coronal emission. The movie reveals that rare flare-like signatures, presumably associated with reconnection, are visible only far from the footpoint area. In the text this is interpreted to mean there is no clear indication of reconnection at visible scales at the footpoint of the bright coronal emission.

Kleint, L., Berkefeld, T., Esteves, M., et al. 2020, A&A, 641, A27, doi: 10.1051/0004-6361/202038208

Kuckein, C., Denker, C., Verma, M., et al. 2017, in Fine Structure and Dynamics of the Solar Atmosphere, ed. S. Vargas Domínguez, A. G. Kosovichev, P. Antolin, & L. Harra, Vol. 327, 20–24, doi: 10.1017/S1743921317000114

Kulsrud, R. M. 2011, Physics of Plasmas, 18, 111201

Lagg, A., Woch, J., Krupp, N., & Solanki, S. K. 2004, A&A, 414, 1109

Leenaarts, J., Golding, T., Carlsson, M., Libbrecht, T., & Joshi, J. 2016, A&A, 594, A104

Leighton, R. B. 1959, ApJ, 130, 366

Leighton, R. B., Noyes, R. W., & Simon, G. W. 1962, ApJ, 135, 474

Lin, H., & Rimmele, T. 1999, ApJ, 514, 448

Liu, Y., Hoeksema, J. T., Scherrer, P. H., et al. 2012, Sol. Phys., 279, 295, doi: 10.1007/s11207-012-9976-x

Nash, A. G., Sheeley, N. R., J., & Wang, Y. M. 1988, Sol. Phys., 117, 359, doi: 10.1007/BF00147253

Nelson, C. J., Freij, N., Bennett, S., Erdélyi, R., & Mathioudakis, M. 2019, ApJ, 883, 115, doi: 10.3847/1538-4357/ab3a54

Osterbrock, D. E. 1961, ApJ, 134, 347

Parker, E. N. 1972, ApJ, 174, 499

Parker, E. N. 1988, ApJ, 330, 474

Pontin, D. I., & Hornig, G. 2020, Living Reviews in Solar Physics, 17, 5, doi: 10.1007/s41116-020-00026-5

Priest, E. R., Chitta, L. P., & Syntelis, P. 2018, ApJL, 862, L24, doi: 10.3847/2041-8213/aad4fc

Priest, E. R., Heyvaerts, J. F., & Title, A. M. 2002, ApJ, 576, 533

Rachmeler, L. A., Bueno, J. T., McKenzie, D. E., et al. 2022, ApJ, 936, 67, doi: 10.3847/1538-4357/ac83b8

Rüedi, I., Keller, C. U., & Solanki, S. K. 1996, Sol. Phys., 164, 265, doi: 10.1007/BF00146639

Schmidt, W., von der Lühe, O., Volkmer, R., et al. 2012, Astronomische Nachrichten, 333, 796, doi: 10.1002/asna.201211725

Schrijver, C. J., Title, A. M., Harvey, K. L., et al. 1998, Nature, 394, 152, doi: 10.1038/28108

Shibata, K., Nakamura, T., Matsumoto, T., et al. 2007, Science, 318, 1591, doi: 10.1126/science.1146708

Stenflo, J. O. 1973, Sol. Phys., 32, 41

Sturrock, P. A. 1968, in IAU Symposium, Vol. 35, Structure and Development of Solar Active Regions, ed. K. O. Kiepenheuer, 471

Title, A. M., & Schrijver, C. J. 1998, in Astronomical Society of the Pacific Conference Series, Vol. 154, Cool Stars, Stellar Systems, and the Sun, ed. R. A. Donahue & J. A. Bookbinder, 345

Uchida, Y., & Kaburaki, O. 1974, Sol. Phys., 35, 451, doi: 10.1007/BF00151968

Van Noort, M., Rouppe Van Der Voort, L., & Löfdahl, M. G. 2005, Sol. Phys, 228, 191, doi: 10.1007/s11207-005-5782-z

Wang, Y. M. 2016, ApJL, 820, L13, doi: 10.3847/2041-8205/820/1/L13

Withbroe, G. L., & Noyes, R. W. 1977, Ann. Rev. Astr. Astrophys., 15, 363